Probing the Impact of Valency on the Routing of Arginine-Rich Peptides into Eukaryotic Cells†

Kim S. Kawamura,‡ Michael Sung,‡ Eleonora Bolewska-Pedyczak, and Jean Gariépy*

Department of Medical Biophysics, University of Toronto, and Ontario Cancer Institute, University Health Network, Toronto, Ontario, Canada

Received July 12, 2005; Revised Manuscript Received October 21, 2005

ABSTRACT: Multivalency represents a critical parameter in cell biology responsible for the overall avidity of low-affinity interactions and the triggering of cellular events. Functions such as catalytic activity, cellular uptake, or localization are frequently linked to the oligomeric state of a protein. This study explores the impact of multivalency on the import and routing of peptides into cells. Specifically, cationic import sequences such as decaarginine, decalysine, and the HIV Tat peptide (GRKKRRQRRRAP, residues 48−59) as well as the nuclear localization sequence from SV40 large T-antigen were assembled into defined peptide oligomers by fusing them to the tetramerization domain of human p53 (residues 325−355, *h*p53^{tet} domain). The resulting tetravalent peptides typically displayed between 10- and 100-fold enhancements in cellular import and intracellular routing properties in relation to their monomeric homologues. These peptides were not toxic to cells. Flow cytometry results and transfection assays indicated that tetravalent decaarginyl peptides (10R-p53^{tet} and NLS-10R-p53^{tet}) were the peptides most efficiently routed into cells. Their mechanism of import was subsequently examined on unfixed, viable cells using a combination of metabolic inhibitors, flow cytometry, and microscopy techniques. These studies revealed that tetravalent arginine-rich peptides bind to heparan sulfate on the cell surface, are internalized at 37 °C, but not at 4 °C, via a clathrin-mediated pathway, and accumulate into endosome-like acidic compartments. A fraction of these tetravalent peptides access the cytosol and accumulate in the nucleus of cells. This study concludes that the oligomerization of proteins harboring arginine-rich peptide chains may profoundly influence their ability to enter and be routed into cells.

Avidity and valency are related concepts in biology. The term avidity is typically defined as the overall strength of a series of molecular interactions and is dependent on both the intrinsic affinity of individual receptor−ligand interactions and the valency or number of such interactions. For instance, events such as cell binding and cell signaling are modulated by the multivalent nature of low-affinity binding events occurring on cell surfaces (*1*, *2*) or inside cells (*3*). These events can be further dissected and defined at a molecular level in terms of the density, arrangement, and dynamics of individual receptor and ligand interactions (*1*). Protein architectures often incorporate multiple protein modules within their primary structure, a design feature that promotes valency effects. Protein templates displaying a modular design for avidity purposes include carbohydrate-binding domains (*4*) as well as cell surface receptors (*5*). In addition, protein templates often aggregate, oligomerize, or self-assemble into multivalent structures harboring unique functional features (*6*−*8*), suggesting that the impact of valency exceeds the limited concept of additive binding events.

Internalization and cellular trafficking events are particularly sensitive to valency effects (*9*). For example, peptides and proteins harboring cell import (cationic domains) and nucleus-routing (nuclear localization signals) sequences display enhanced routing functions upon adopting a multivalent quaternary structure. One case in point is nucleoplasmin, a protein that mediates nucleosome assembly. Nucleoplasmin self-associates into pentamers, and its accumulation in the cell nucleus is linked to the number of nuclear localization signals (NLS)[1] present within its pentameric structure (*10*). Similarly, the routing of the tumor suppressor protein p53 in and out of the nucleus is linked to its tetrameric state (*11*, *12*). Finally, the number of NLS sequences linked to a non-nuclear protein such as bovine serum albumin dictates the level of nuclear uptake of the resulting conjugates (*13*, *14*). The effect of multivalency on the cellular import of cationic peptides (also termed protein transduction domain or PTD) and polymers is also remarkable. Covalently assembled, polyvalent cationic peptides have been shown to dramatically enhance the import of macromolecules into cells (*9*, *15*), a feature that strongly supports the known correlation between molecular size and the

† This study was funded by the Canadian Breast Cancer Research Alliance.

* To whom correspondence should be addressed: Ontario Cancer Institute, 610 University Ave., Toronto, ON M5G 2M9, Canada. Telephone: (416) 946-2967. Fax: (416) 946-6529. E-mail: gariepy@uhnres.utoronto.ca.

‡ These authors contributed equally to this study.

[1] Abbreviations: *h*p53^{tet}, human p53 tetramerization domain; CHO, Chinese hamster ovary; eGFP, enhanced green fluorescence protein; NLS, nuclear localization sequence(s); PTD, protein transduction domain; TEM, transmission electron microscopy; SOD, superoxide dismutase; Vero, African green monkey kidney epithelial cells.

10.1021/bi051338e CCC: $33.50
Published on Web 01/10/2006

transport of cationic peptides and polymers into cells (*16*). Mechanistically, cationic peptides have been shown to enter cells by clathrin-mediated endocytosis (*17*−*19*) and, in the case of Tat−EGFP fusion proteins, by exploiting a caveolar pathway (*20*, *21*). Macropinocytosis has also been recently proposed as an alternate import mechanism for a Tat−Cre fusion protein (*22*, *23*). Macropinocytosis has been linked to the engulfing and import of particles into cells, including large entities such as viruses (*24*) and bacteria (*25*, *26*). The aggregation state of PTDs with their cargo may thus influence the macroscopic state of such complexes and may in turn result in more than one internalization pathway being operative as in the case of entry of HIV into cells (*27*). The nature of the aggregation state of a PTD-containing molecular complex must thus be determined to assess the dominant mechanism regulating their import into cells.

This study examines how the oligomerization state of cationic peptides through their fusion to a self-assembling peptide motif can effectively enhance their import and cell routing properties. More precisely, peptides were designed to spontaneously assemble in solution into discrete tetramers (rather than molecular aggregates) as a result of linking short cationic peptide sequences in combination with the SV40 large T-antigen nuclear localization sequence (NLS) to the N-terminus of the human tetramerization domain of p53 (*h*p53^{tet}, residues 325−355). Results presented in the study demonstrate that the transduction or import properties of the resulting cationic peptide tetramers can be enhanced by 1 or more orders of magnitude in relation to those of their respective monomeric peptide analogues [homologues harboring a single L344P point mutation within their p53^{tet} domain (*28*)]. Thus, the important gain in functional properties associated with the oligomerization of such peptides can be assigned to valency effects on established cell routing mechanisms.

EXPERIMENTAL PROCEDURES

Materials. The metabolic inhibitors monodansylcadaverine, nystatin, and cytochalasin D, sucrose, and poly-L-lysine (MW_{av} = 25 kDa) and FITC-labeled anti-mouse IgM were purchased from Sigma-Aldrich (Oakville, ON). Chamber slides were bought from Lab-Tek (Nalge Nunc International). LysoTracker Red was purchased from Molecular Probe (Invitrogen), while the colloidal gold−streptavidin conjugate was obtained from British Biocell International (Cardiff, U.K.). Anti-heparan sulfate mouse IgM was bought from Sikagaku Corp. (Tokyo, Japan).

Cell Lines. Chinese hamster ovary cells (CHO) and African green monkey kidney epithelial cells (Vero) were obtained from ATCC (Rockville, MD) and were maintained in α-MEM supplemented with 10% fetal calf serum and antibiotics in the presence of 5% CO_2. The CHO cell line pgs A-745 does not produce proteoglycans due to a lack of xylosyltransferase, an enzyme necessary for initiation of glycosaminoglycan synthesis (*29*). The CHO cell line pgs D-677 harbors a single mutation that abolishes both *N*-acetylglucosaminyltransferase and glucuronosyltransferase activities which are crucial for the polymerization of heparan sulfate (HS) disaccharide chains and therefore does not produce HS proteoglycans (*30*). These two mutated CHO cell lines were also obtained from ATCC and were maintained in Ham's F-12K medium adjusted to 1.5 g/L sodium bicarbonate, supplemented with 10% fetal calf serum and antibiotics. All cell lines were grown at 37 °C in the presence of 5% CO_2.

Synthesis, Fluorescein Labeling, and Biotinylation of hp53^{tet} Peptides. Peptides were synthesized on an Applied Biosystems 431A synthesizer using 9-fluorenylmethoxycarbonyl (Fmoc) chemistry and RINK amide resin (Applied Biosystems, Mississauga, ON). After the final deprotection step, the resin samples were split to label the N-terminus of peptides with either fluorescein [6-carboxyfluorescein (6-FAM), Molecular Probes/Invitrogen Canada, Burlington, ON] or biotin using standard active ester (HBTU) chemistry. Peptides were cleaved from their support by resuspending each resin in TFA, phenol, water, thioanisole, and ethanediol (82.5, 5, 5, 5, and 2.5%, respectively). The reaction was allowed to proceed for 2 h. Arginine-containing peptides were cleaved for an additional 1 h for each arginine residue present in their sequence up to a maximum of 6 h. The cleaved peptides were precipitated in ice-cold ether and spun for 5 min at 1500 rpm (Sorvall). The pellets were then resuspended in 5 mL of water and lyophilized. Purification of the crude peptide products was performed on a C_4 semipreparative reverse phase column (200 mm × 20 mm, Waters, Milford, MA). Peptides dissolved in a 0.1% (v/v) TFA/water mixture (mobile phase) were loaded onto the column equilibrated in the same mobile phase and separated using a 5 to 80% acetonitrile gradient over a 30 min period. The flow rate of the column was 7 mL/min. Peptide masses were confirmed by mass spectrometry, and their purity was established by analytical reverse phase chromatography (C_{18}, 200 mm × 5 mm, Waters; Supporting Information).

Cell Viability Assay. Cell viability as a function of peptide concentration was measured using the tetrazolium salt WST-1 {4-[3-(4-iodophenyl)-2-(4-nitrophenyl)-2*H*-5-tetrazolio]-1,3-benzenedisulfonate, Boehringer Mannheim}. Briefly, CHO cells resuspended in α-MEM containing 10% fetal calf serum were seeded in a 96-well plate (3×10^5 cells/well) overnight. The next day, the cells were exposed to peptides containing media with peptide concentrations ranging from 0 to 25 μM at 37 °C for 4 h. The cells were then washed with PBS, and their viability was assessed by adding WST-1 dissolved in PBS (100 μL, 10%, v/v) to each well and incubated for 1 h at 37 °C before the absorbance of each well was read. The percent viability of cells was derived from absorbance readings measured at 460 nm for peptide-treated cells in relation to samples of untreated CHO cells. Data (Supporting Information) represent mean percent viability values based on experiments performed in triplicate.

Cross-Linking Studies. Samples of purified peptides (25 μM) were resuspended in 0.2% glutaraldehyde in phosphate buffer [25 mM, with 200 mM NaCl (pH 7.0)] and incubated at room temperature for 20 min. Sample aliquots (20 μL) were then mixed with SDS−PAGE sample buffer [10% (v/v) glycerol, 62.5 mM Tris-HCl (pH 6.8), and 2% w/v SDS] and boiled and the cross-linked peptide species resolved using 15% SDS−PAGE. Protein bands were revealed by staining the gel with Coomassie Brilliant Blue. The presence of a tetrameric species qualitatively yields a ladder of protein bands representing the monomeric, dimeric, trimeric, and tetrameric species of the monomeric peptide.

Gel Filtration Analysis. The oligomeric state of each *h*p53^{tet} peptide was also analyzed by gel filtration chromatography on a Superdex 75 column (10 mm × 30 mm, Amersham Biosciences). The column was equilibrated in phosphate buffer [25 mM phosphate and 200 mN NaCl (pH 7.0)] and was calibrated with established protein standards and control *h*p53^{tet} peptides as previously described (*31*). The flow rate was 1 mL/min. The elution volume (retention time) associated with each *h*p53^{tet} peptide (100 μM, 400 μL loaded in phosphate buffer) confirmed their monomeric or tetrameric state.

Analytical Ultracentrifugation. Sedimentation equilibrium ultracentrifugation experiments were performed on a Beckman Optima XL-I analytical ultracentrifuge using an AN50-Ti rotor with six-channel charcoal Epon cells as previously described (*31*). Average mass estimates were derived from data fitted using a single-species model.

Time-Dependent Internalization of hp53^{tet} Peptides into Eukaryotic Cells. CHO and Vero cells (1×10^6 cells/mL) were resuspended in α-MEM containing 10% fetal calf serum and incubated with 6-FAM-labeled peptides (0.5 μM each) over a period of 6 h at 37 °C. The relative mean fluorescence signal of any given cell population was determined by flow cytometry (FACscan, Becton Dickinson). Measured events were gated on the population of viable cells present within each cell sample using the cell impermeant DNA intercalating dye, 7-AAD (0.1 mg/mL). Data represent the mean relative fluorescence signal based on experiments performed in triplicate.

Effects of Metabolic Inhibitors and Polylysine on Peptide Internalization. CHO and Vero cells (1×10^6 cells/mL) were treated in hypertonic medium (0.4 M sucrose) with monodansylcadaverine (100 μM), nystatin (25 μg/mL), cytochalasin D (5 μM), or poly-L-lysine (MW_{av} = 25 kDa, 2 μM) for 30 min at 37 °C before incubation with 6-FAM-labeled peptides (0.5 μM) in α-MEM containing 10% fetal calf serum. Both cell lines were also incubated at 4 °C for 30 min prior to addition of peptides to establish the role of temperature in the internalization process. The effects of these conditions on the time-dependent internalization of peptides were monitored in terms of a change in mean fluorescence values recorded by flow cytometry on the viable cell population. Data represent the mean relative fluorescence signal based on experiments performed in triplicate.

Role of Heparan Sulfate Production in Peptide Internalization. The levels of heparan sulfate on the surface of mutant CHO cell lines pgsA-745 and pgsD-677 as well as wild-type CHO cells were initially characterized by flow cytometry. Briefly, cells were detached from flasks with trypsin and resuspended in medium. Trypsin treatment was limited to 30 s, a period of time that led to no measurable decrease in the level of cell surface heparan sulfate proteoglycan on wild-type CHO cells (as monitored with an anti-heparan sulfate mouse IgM). The antibody (1:200) was mixed with 0.5×10^6 cells of each cell line at 4 °C for 1 h. The cell samples were then washed three times with cold PBS containing 0.5% (w/v) BSA, labeled with FITC anti-mouse IgM (1:150 dilution, 1 h, 4 °C), and analyzed by flow cytometry. All three cell lines were subsequently incubated with both the tetrameric and monomeric fluorescein-labeled 10K-p53^{tet} peptides at 37 °C for 2 h and analyzed by flow cytometry to determine the level of internalization of each peptide in different cell lines.

Confocal Microscopy. Aliquots of CHO and Vero cell suspensions (5×10^4 cells/mL) were dispensed into four-well coverglass slides (chamber slides, Lab-Tek), and cells were allowed to adhere for 18 h. The cells were then incubated for up to 6 h at 37 °C with 1 μM 6-FAM-labeled peptides prepared in medium. The peptide-containing medium was then removed from the slide wells at different time intervals, and the adherent cells were washed twice with ice-cold PBS containing 0.1% (w/v) BSA prior to visualization of the field of labeled cells using a Zeiss Two Photon Confocal (Meta) microscope equipped with an argon laser. Images of adherent cells (1 μm thick) were recorded as well as their corresponding phase contrast images (DCI channel).

Localization of Peptides in Endocytic Vesicles. Adherent CHO and Vero cells (5×10^4 cells/mL) grown in chamber slides were co-incubated for 30 min at 37 °C with 6-FAM-labeled peptides (1 μM) and LysoTracker Red (75 nM, a fluorescent dye which labels acidic vesicles from Molecular Probes). The comigration of peptides and dye inside cells was assessed by confocal microscopy (argon−helium lasers).

Transmission Electron Microscopy. Resuspended CHO cells (1×10^6 cells/mL; α-MEM, 10% FCS) were incubated for either 30 min or 3 h at 37 °C in the presence or absence of biotinylated 10R-p53^{tet} peptides (1 μM) prepared in cell medium. The cells were then harvested and fixed for 3 h in room temperature in phosphate buffer (pH 7.2) containing 4% (v/v) paraformaldehyde and 0.5% (v/v) glutaraldehyde. The cells were subsequently harvested, cooled at 4 °C, washed with PBS buffer, stained with OsO_4 [1% (w/v) OsO_4 in cacodylate buffer (pH 7.4)], dehydrated under ethanol, and embedded in LRWhite plastic. Thin sections of embedded cells were deposited onto nickel grids and stained for 30 min with 15 nm colloidal gold−streptavidin conjugate dissolved in PBS. The grids were washed once with 1% (w/v) BSA in PBS and five times with sterile distilled water droplets (30 μL/drop) for 10 min. The grids were also counterstained with 5% uranyl acetate and finally mounted on a Hitachi H600 transmission electron microscope (Hitachi Scientific Instruments, Mountain View, CA).

Gel Retardation Assay. Increasing amounts of peptides (0−5 μg) were mixed in PBS with 1 μg of plasmid DNA (pEGFPLuc, Clontech) for 10 min at room temperature to determine the minimal weight ratio of peptide to plasmid needed to fully condense plasmid DNA (retard its migration in agarose gels). Peptide−plasmid complexes were then loaded onto 0.8% agarose gels (stained with ethidium bromide) and electropherically resolved at 100 V. DNA bands were visualized with a UV light and photographed (Supporting Information).

Transfection Experiments. Peptide−plasmid DNA complexes were prepared by mixing 4 μg of pEGFPLuciferase plasmid (Clontech) with an optimized amount of peptides (60−100 μg) in PBS to a final volume of 50 μL. The complexes were allowed to form for 20 min at room temperature. CHO cells (1×10^6 cells/mL) were then harvested and added directly to the tube containing the DNA−peptide complexes, and the final volume was adjusted to 500 μL. The cells were incubated at 37 °C for 4 h before being transferred to six-well plates (Nunc) containing 4.5 mL of medium/well. Transfected cells were grown for 48 h

A.

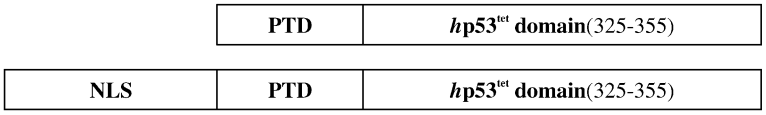

B.

Acronym	Peptide sequence	M.W. (monomer)
10K-p53^{tet}	**K**$_{10}$GEYFTLQIRGRERFEMFRELNEALELKDAQA	5.04 kDa
NLS-10K-p53^{tet}	APPKKKRKVEDP**K**$_{10}$GEYFTLQIRGRERFEMFRELNEALELKDAQA	6.41 kDa
10K-p53^{mono}	**K**$_{10}$GEYFTLQIRGRERFEMFRE**P**NEALELKDAQA	5.02 kDa
NLS-10K-p53^{mono}	APPKKKRKVEDP**K**$_{10}$GEYFTLQIRGRERFEMFRE**P**NEALELKDAQA	6.40 kDa
10R-p53^{tet}	**R**$_{10}$GEYFTLQIRGRERFEMFRELNEALELKDAQA	5.32 kDa
NLS-10R-p53^{tet}	APPKKKRKVEDP**R**$_{10}$GEYFTLQIRGRERFEMFRELNEALELKDAQA	6.69 kDa
10R-p53^{mono}	**R**$_{10}$GEYFTLQIRGRERFEMFRE**P**NEALELKDAQA	5.30 kDa
NLS-10R-p53^{mono}	APPKKKRKVEDP**R**$_{10}$GEYFTLQIRGRERFEMFRE**P**NEALELKDAQA	6.68 kDa
TAT-p53^{tet}	**GRKKRRQRRRAP**GEYFTLQIRGRERFEMFRELNEALELKDAQA	5.31 kDa
NLS-TAT-p53^{tet}	APPKKKRKVEDP **GRKKRRQRRRAP**GEYFTLQIRGRERFEMFRELNEALELKDAQA	6.68 kDa
TAT-p53^{mono}	**GRKKRRQRRRAP**GEYFTLQIRGRERFEMFRE**P**NEALELKDAQA	5.72 kDa
NLS-TAT-p53^{mono}	APPKKKRKVEDP **GRKKRRQRRRAP**GEYFTLQIRGRERFEMFRE**P**NEALELKDAQA	6.66 kDa

FIGURE 1: Schematic representation of p53^{tet} peptides prepared for this study. (A) The tetramerization domain of human p53 is defined by residues 325−355. The PTD (protein transduction domain) was either a decalysyl, a decaarginyl, or the arginine-rich HIV Tat import sequence. The nuclear localization sequence (NLS) chosen represented residues 124−135 of the SV40 large T-antigen. (B) List of sequences, molecular masses and acronyms of all synthetic peptides cited in this study. The superscript after each peptide name indicates their oligomerization state under physiological conditions (tet, tetramer; mono, monomer).

at 37 °C prior to assaying for luciferase activity (Promega kit, Promega, Madison, WI). Briefly, cells were layered with a cell lysis buffer [25 mM Tris-phosphate (pH 7.8), 2 mM DTT, 2 mM 1,2-diaminocyclohexane-*N*,*N*,*N*′,*N*′-tetraacetic acid, 10% glycerol, and 1% Triton X-100] and harvested from the plates. The samples were then vortexed and subjected to freezing and thawing. The cell debris was removed by centrifugation (14 000 rpm for 2 min). The luciferase activity was determined using luciferin (Promega Assay reagent, Promega), and light units were read on a luminometer (Lumat LB 9507, Berthold, Princeton, NJ). Relative light units (RLU) were standardized to RLU per milligram of protein. The protein concentration of each sample was determined using a Bradford assay (Bio-Rad). Cells transfected with pGeneGrip (Gene Therapy System, San Diego, CA) were stained for β-galactosidase using a commercial kit (β-gal staining kit, Roche).

RESULTS

Design and Tetramerization of hp53^{tet}-Based Self-Assembling Peptides. The objective of this study was to explore the concept and effect of multivalency on the mechanisms of cellular import and intracellular localization of cationic peptides in eukaryotic cells. To evaluate this concept, cationic peptides were designed to exist in either a monomeric or in a defined oligomeric state. The tetramerization domain of human p53 (*h*p53^{tet}) represents a well-characterized oligomerization motif (*32*−*34*) that was used in the study presented here to self-assemble and effectively display distinct functional routing domains on a tetravalent peptide template. More precisely, the minimal *h*p53^{tet} tetrameric domain stretches from residue 325 to 355 and can be described as a symmetric dimer of dimers (*35*, *36*). The elements of secondary structure present in the *h*p53^{tet} motif consist of a β-strand (residues 326−334) followed by a turn region (residues 335 and 336) and ending with an α-helical segment (residues 337−354). Two *h*p53^{tet} domains associate to form an antiparallel dimer which then forms a tetramer with another *h*p53^{tet} dimer along the interface of their α-helical domains. Tetramers are stabilized by hydrophobic interactions between both the primary dimer and the dimer−dimer interface as shown by mutational studies on hydrophobic residues (*37*, *38*). Electrostatic interactions have also been shown to play a role (*31*). However, a single mutation at leucine 344 to proline (L344P) abolishes tetramer formation (*28*), a feature that enabled us to construct the corresponding monomeric versions of our cationic peptides (Figure 1). Cellular import and intracellular routing were encoded into the peptides by introducing known protein transduction domains (PTDs) and a nuclear localization sequence (NLS) at the N-terminus of our *h*p53^{tet} peptides. Three different IS peptide sequences were evaluated in terms of their effectiveness in routing the *h*p53^{tet} scaffolds into eukaryotic cells: decalysine (10K), decaarginine (10R), and the Tat import sequence (GRKKRRQRRRAP) (*39*). The selected NLS sequence was a peptide domain derived from the SV40 large T-antigen (*40*) and was shown to effectively direct proteins to the cell nucleus (*13*, *39*). The complete list of peptides designed for this study is presented in Figure 1. Their monomeric and tetrameric states were confirmed using a combination of methods which included analytical ultracentrifugation, gel permeation chromatography, and

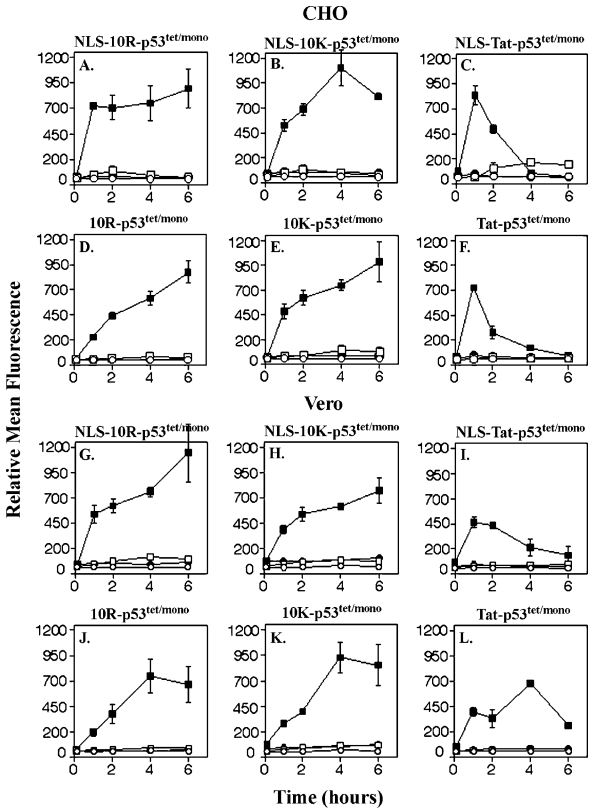

FIGURE 2: Time-dependent internalization of fluorescein-labeled p53$^{tet/mono}$ peptides into CHO and Vero cells as measured by flow cytometry. (A−F) CHO cells were exposed to fluorescein-labeled p53$^{tet/mono}$ peptides (0.5 μM) for time periods of up to 6 h. Incubations were performed at 4 and 37 °C. (G−L) Vero cells were exposed to fluorescein-labeled p53$^{tet/mono}$ peptides (0.5 μM) at 4 and 37 °C for time periods of up to 6 h. In all panels, curves represent the time-dependent changes in relative mean fluorescence intensity for cells exposed to fluorescent tetrameric p53^{tet} (■ and ●) and monomeric p53^{mono} (□ and ○) peptides incubated at 37 (■ and □) and 4 °C (● and ○). All data points represent the average relative mean fluorescence signals from sets of experiments performed in triplicate.

glutaraldehyde cross-linking/SDS−PAGE analyses (data not shown) as described elsewhere (*31*). In particular, all *h*p53^{tet} mutants harboring a L344P substitution were shown to be monomeric.

The Multivalent Display of Short Cationic Peptides within the Context of hp53^{tet} Peptides Promotes Their Import into Mammalian Cells. The impact of multivalency on cellular import was first established by comparing the levels of cellular uptake of monomeric (L344P variants) versus tetrameric p53^{tet}-based peptides. The valency effect was monitored for peptides harboring one of three types of cationic import sequences (PTD) at their N-terminus (either a decalysine, decaarginine, or the HIV Tat sequence). A subset of peptides also included the cationic SV40 large T-antigen NLS sequence (Figure 1). All peptides were labeled with fluorescein (6-FAM), and their uptake into CHO and Vero cells was analyzed by flow cytometry [relative mean fluorescence (RMF) units]. The internalization of monomeric and tetrameric peptides was monitored as a function of time and temperature (4 and 37 °C) and was presented in terms of the molar concentration of cationic import peptides within each construct (Figure 2). Three salient points emerged from the study. (1) The import of p53^{tet} peptides into cells is blocked at 4 °C. (2) Tetrameric peptides are dramatically more effective at entering CHO or Vero cells than their monomeric counterparts. (3) Decaarginine and decalysine transduction sequences are more efficient than the arginine-rich HIV Tat import sequence in terms of the levels of cellular uptake observed in both cell lines and cellular retention over a period of 6 h. More specifically, endocytic events in eukaryotic cells are typically inhibited at 4 °C (*41*). Cell surface binding of p53^{tet} peptides can thus be assessed at 4 °C by flow cytometry and differentiated from surface-bound and internalized peptides occurring at 37 °C. The extent of cellular uptake for monomeric p53^{tet} peptides at 37 °C reached a plateau of 50−150 RMF units in CHO and Vero cells over a 6 h incubation period. The import of tetrameric p53^{tet} peptides into such cells, however, typically gave RMF values on the order of 700 and 1200, with the exception of Tat-containing p53^{tet} peptides, where both cell lines rapidly internalized such peptides, but started to display a sharp decline in intracellular fluorescence intensity after 1 h (Figure 2C,F,I,L). The profiles of uptake of Tat-containing p53^{tet} peptides into CHO and VERO cells correlate with a recent study of the import and retention profiles of Antp, nonaarginine, and Tat peptides in MC57 cells (*42*). More specifically, Tat peptides appear to be less efficient at entering cells and are either degraded or exocytosed more efficiently than other import sequences. Finally, the presence of a cationic NLS sequence within p53^{tet} peptides provided in some cases a small enhancement in cellular uptake (Figure 2A,D,G,J). Interestingly, the cationic NLS-p53^{tet} peptide lacking a PTD domain was not imported into CHO cells, suggesting that the APPKKKRKVEDP sequence by itself is not sufficient to act as a PTD (Supporting Information).

Tetrameric p53^{tet} Peptides Can Condense and Deliver Plasmid DNA into Cells. The importance of valency with respect to cellular uptake was also confirmed using a functional assay. More precisely, p53^{tet} peptides were used to condense and transfer plasmid DNA (pEFGPLuciferase, pGeneGrip) into CHO cells (Figure 3). These plasmids encode the expression of reporter enzymes, namely, luciferase (pEFGPLuciferase) and β-galactosidase (pGeneGrip). The condensation event occurs spontaneously as a result of noncovalent interactions between the DNA polyanionic phosphate backbone and cationic p53^{tet} peptides. Gel retardation assays were initially performed to evaluate the peptide:plasmid DNA ratios needed to fully complex the peptides with plasmid DNA (Supporting Information). Briefly, increasing amounts of peptides were mixed with 1 μg of plasmid DNA, and the resulting complexes were electrophoretically resolved in agarose gels. The shifting of the plasmid DNA band to the top of the gel indicated condensation. Peptide:DNA weight ratios between 2:1 and 2.5:1 were sufficient to complex DNA with either monomeric or tetrameric p53^{tet} peptides. As presented in Figure 3, the tetrameric forms of NLS-10R-p53^{tet}, 10R-p53^{tet}, and NLS-10K-p53^{tet} complexed with either pEFGPLuciferase or pGeneGrip displayed the highest levels of luciferase (logarithmic scale; $>10^7$ RLU/mg of protein) and β-galactosidase (blue-colored cells) activity (Supporting Information). Specifically, tetrameric peptides carrying either a 10-lysine or a 10-arginine domain yielded luciferase signals that were between 20- and 1000-fold higher in value than their

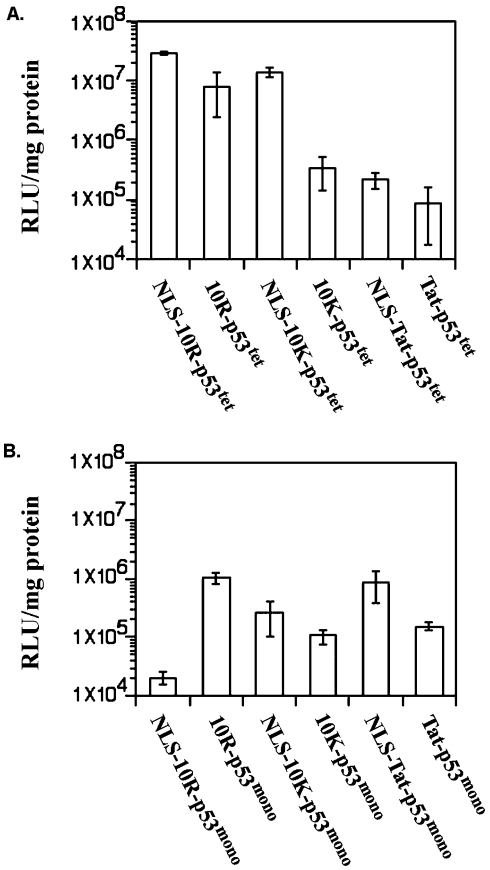

FIGURE 3: Comparison of transfection efficiencies between p53$^{tet/mono}$ peptides complexed with plasmid DNA. The pEGFPLuciferase plasmid was condensed with p53^{tet} peptides, and the complexes were used to transfect CHO cells. (A) Luciferase expression levels [relative light units (RLU) per milligram of protein] for CHO cells transfected with tetrameric peptide−plasmid DNA complexes (see Experimental Procedures). (B) Luciferase expression levels for CHO cells transfected with monomeric peptide−DNA complexes. Baseline readings for CHO cells or CHO cells transfected with DNA alone ranged in value from 0 to 10^3 RLU. Histogram bars represent the average RLU signals from sets of experiments performed in triplicate.

respective monomeric counterparts (Figure 3). Only in the case of NLS-10K-p53^{tet} in relation to 10K-p53^{tet} did the addition of an NLS sequence yield a significant increase (>10-fold) in luciferase activity. Interestingly, the luciferase signals observed for the Tat-containing p53^{tet} peptides appeared to be lower in all cases and independent of the valency of these peptides (Figure 3).

Decaarginine-Containing p53^{tet} Peptides Enter Cells by Clathrin-Mediated Endocytosis. The preceding analysis of cationic import sequences (Figures 2 and 3) defined tetrameric p53^{tet} peptides containing a 10-arginine transduction domain (10R-p53^{tet} and NLS-10R-p53^{tet}) as the sequences most efficient at entering both CHO and Vero cells and at delivering plasmid DNA into CHO cells. A study was subsequently initiated to delineate cellular events linked to the mechanisms of cell entry and intracellular routing of these decaarginine p53^{tet} peptides. These p53^{tet} peptides were not internalized by cells at 4 °C (Figure 2). Their mechanism of cell entry was further examined using inhibitors of endocytosis. First, CHO and Vero cells were treated with either monodansylcadaverine (MDC), an inhibitor known to block the formation of clathrin-coated pits (*43*−*45*), or incubated

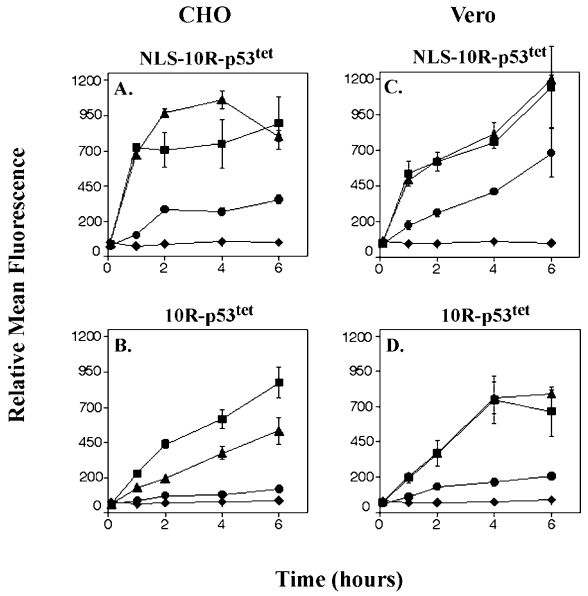

FIGURE 4: Possible role of clathrin and caveolae in the mechanism of cellular import of decaarginine-containing p53^{tet} peptides into CHO and Vero cells. Both cell lines were incubated in the presence of fluorescein-labeled peptide (0.5 μM) at 37 °C for a time period of up to 6 h under four different conditions: in the absence of inhibitors (■) and in the presence of either 100 μM monodansylcadaverine (●), 25 μg/mL nystatin (▲), or 0.4 M sucrose (◆). All data points represent the average relative mean fluorescence signals from sets of experiments performed in triplicate.

in a hypertonic medium (0.4 M sucrose), a condition that also inhibits clathrin-mediated endocytosis (*46*−*48*). These conditions were established before and during the incubation step with the decaarginine-containing p53^{tet} peptides. The time-dependent entry of fluorescein-labeled NLS-10R-p53^{tet} and 10R-p53^{tet} into CHO and Vero cells was monitored by flow cytometry and indicated that peptide internalization into both cell lines was inhibited under hypertonic conditions at 37 °C (Figure 4A−D). Similarly, the extent of import of peptide into cells exposed to MDC (100 μM) was significantly reduced by 70−80% relative to that in untreated cells (Figure 4A−D). The import of decaarginine-based p53^{tet} peptides into cells may also be linked to a caveolae-mediated internalization process. Nystatin, a cholesterol depletion agent (*48*, *49*), was thus used to inhibit caveolae formation in CHO and Vero cells. Nystatin treatment (25 μg/mL) of Vero cells did not affect the import of either NLS-10R-p53^{tet} and 10R-p53^{tet} peptides (Figure 4C,D) and only partially reduced the level of internalization of 10R-p53^{tet} peptides (approximately 40%) into CHO cells (Figure 4B). Interestingly, the entry of NLS-10R-p53^{tet} into CHO cells was actually enhanced by the presence of this inhibitor (Figure 4A). These studies would suggest that such p53^{tet} peptides enter cells by clathrin-mediated endocytosis. The actin cytoskeleton serves an important role in vesicular transport and may be linked to the import of arginine-containing p53^{tet} peptides. CHO and Vero cells were thus treated with cytochalasin D (2.5 μM), a microfilament disrupting agent (*50*, *51*) that specifically depolymerizes F-actin, to examine the role of microfilaments in transduction of peptide into cells. The concomitant administration of cytochalasin D with either peptide to cells inhibited significantly their internalization into CHO (Figure 5B, 10R-p53^{tet}, ∼70% reduction) and Vero cells (Figure 5C,D, 10R-p53^{tet} and NLS-10R-p53^{tet}, 40−50% reduction).

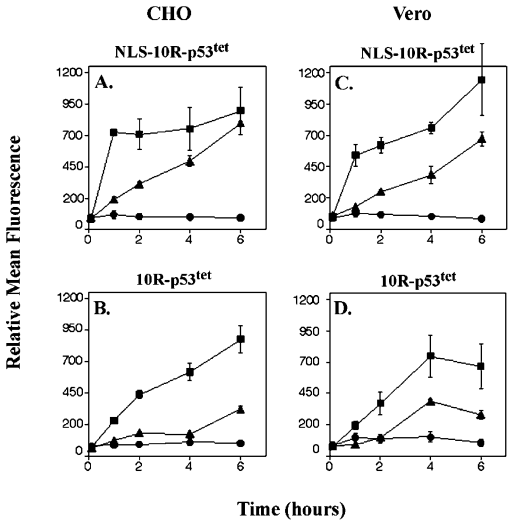

FIGURE 5: Role of microfilaments and polycationic charges on the uptake of decaarginine-containing p53^{tet} peptides into CHO and Vero cells. Both cell lines were incubated in the presence of fluorescein-labeled peptide (0.5 μM) at 37 °C for a time period of up to 6 h under three different conditions: in the absence of inhibitors (■) and in the presence of either 2 μM poly-L-lysine (●) or 5 μM cytochalasin D (▲). All data points represent the average relative mean fluorescence signals from sets of experiments performed in triplicate.

Surprisingly, the uptake of NLS-10R-p53^{tet} by CHO cells was not blocked by cytochalasin D but rather simply delayed by more than 5 h in relation to that in untreated CHO cells (absence of cytochalasin D).

Defining the Nature of Surface Receptors Recognized by Tetrameric Arginine-Containing Peptides. Poly-L-lysine is a cationic poly-amino acid peptide chain that has been shown to bind to anionic sites on the cell surface (*15*, *16*, *52*−*54*). The addition of polylysine (MW_{av} = 25 kDa; 2 μM) to the cell medium of CHO and Vero cells completely inhibited the internalization of arginine-rich peptides 10R-p53^{tet} and NLS-10R-p53^{tet} (Figure 5A−D), suggesting that these peptides interact with a common class of anionic ligands masked by the cationic charges present on poly-L-lysine.

Cell surface glycosaminoglycans such as heparan sulfate have been implicated in the binding of short cationic peptides such as the HIV Tat import sequence, penetratin, and nonaarginine peptides to cells (*52*, *55*). Glycosaminoglycans may therefore represent a class of anionic surface receptors targeted by 10R-p53$^{tet/mono}$ peptides. To test this hypothesis, the import of fluorescein-labeled 10R-p53^{tet} peptides was assessed in two mutant CHO cell lines, termed pgsA-745 and pgsD-677. These CHO cell lines are unable to produce glycosaminoglycans (*29*) and heparan sulfate (*30*), respectively. The presence or absence of heparan sulfate on the surface of wild-type CHO cells and the CHO cell line variants pgsA-745 and pgsD-677 was confirmed by flow cytometry using an anti-heparan sulfate mouse IgM (*53*). The flow cytometry histograms presented in Figure 6A illustrate that both CHO cell lines pgsA-745 and pgsD-677 did not express heparan sulfate on their surface in contrast to wild-type CHO cells. The role of glycosaminoglycans, and specifically heparan sulfate, in the import of 10R-p53^{tet} peptides into CHO cells was subsequently assessed by flow cytometry. Briefly, tetrameric and monomeric decaarginyl p53 peptides were incubated with the wild-type or mutant

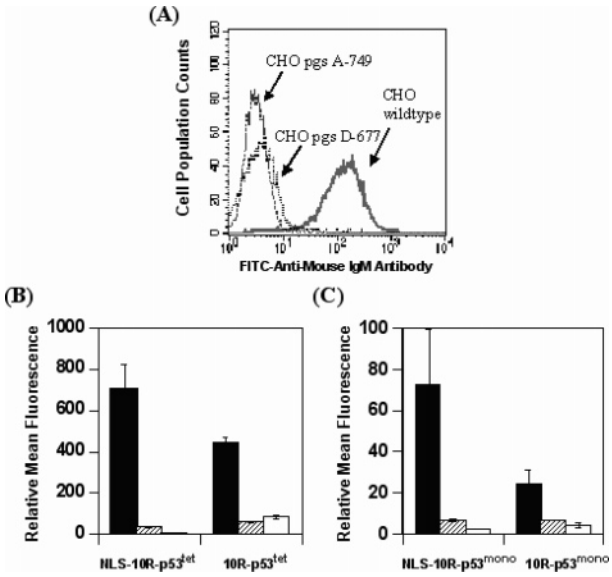

FIGURE 6: Heparan sulfate on CHO cells acts as a receptor for 10R-p53$^{tet/mono}$ peptides. (A) The level of expression of heparan sulfate on the surface of CHO, CHO pgsA-745, and CHO pgsD-677 cells was determined by flow cytometry. Only the wild-type CHO cell line was found to express herapan sulfate as revealed using an anti-heparan sulfate antibody. (B) Histogram depicting the level of internalization of fluorescein-labeled tetrameric 10R-p53^{tet} peptides into CHO, CHO pgsA-745, and CHO pgsD-677 cells after a 2 h incubation at 37 °C as monitored by flow cytometry. (C) Histogram as outlined in panel B with the exception that cells were treated with monomeric forms of fluorescein-labeled 10R-p53^{tet} peptides. In panels B and C, the level of peptide import into cells correlates with the observed mean fluorescence signals: wild-type CHO (black bars), pgs A-745 (hatched bars), and pgs D-677 (white bars), Note that the scale on the relative fluorescence axis (*Y* axis) is 10 times smaller than that in panel B. Histogram bars represent the average relative mean fluorescence signals from sets of experiments performed in triplicate.

CHO cell lines at 37 °C. The relative fluorescence intensities for either tetrameric (Figure 6B) and monomeric 10R-p53^{tet} peptides (Figure 6C) were recorded after 2 h for all three cell lines. As expected, the fluorescence signals observed for the tetrameric peptide variants were typically 1 order of magnitude greater than those of their monomeric homologues (Figure 6B,C). Nevertheless, none of the p53^{tet} peptides were able to enter either the glycosaminoglycan-deficient or the heparan sulfate-deficient CHO cell lines after incubation for 2 h. These results suggest that glycosaminoglycans serve as surface receptors for 10R-p53^{tet} and NLS-10R-p53^{tet} peptides with heparan sulfate, in particular, acting as a receptor that mediates their binding to CHO cells and subsequent internalization. Finally, both monomeric and tetrameric forms of 10R-p53^{tet} and NLS-10R-p53^{tet} bind in a similar fashion to CHO cells (Figure 6B,C).

Decaarginyl p53^{tet} Peptides Localize in Endocytic Vesicles. The intracellular routing of 10R-p53^{tet} and NLS-10R-p53^{tet} in unfixed, viable CHO and Vero cells was assessed by confocal microscopy and transmission electron microscopy. Cells examined by confocal microscopy were also labeled with LysoTracker Red, a fluorescent dye that accumulates in acidic compartments. This organelle marker was used to trace if peptides reached acidic vesicles. The colocalization of fluorescein-labeled peptides and LysoTracker Red (yellow colored areas) was observed by confocal microscopy as a result of an overlap between green and red fluorescence

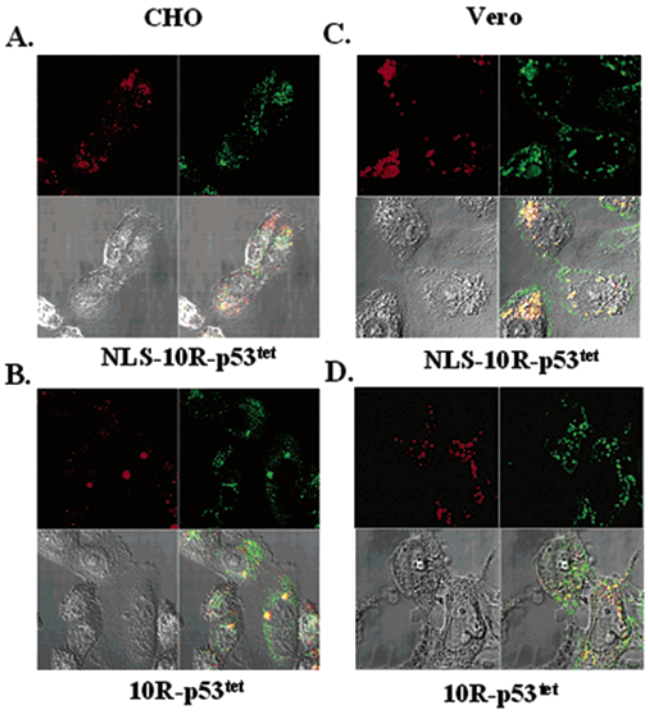

FIGURE 7: 10R-p53^{tet} peptides localize into acidic vesicles after internalization into CHO and Vero cells. (A and B) Confocal images showing the colocalization of fluorescein-labeled NLS-10R-p53^{tet} and 10R-p53^{tet} (1 μM) peptides with LysoTracker Red (75 nM), an acidic vesicle dye, inside vesicular compartments after co-incubation for 40 min with unfixed, viable CHO cells. (C and D) Colocalization of LysoTracker Red and fluorescein-labeled NLS-10R-p53^{tet} and 10R-p53^{tet} (1 μM) peptides after incubation with unfixed, viable Vero cells. Each panel consists of four sections from the same field of view. Clockwise from top left: LysoTrack Red staining, fluorescein-labeled peptide (green color), phase contrast, and composite image.

signals. Both NLS-10R- and 10R-p53^{tet} peptides were observed to comigrate with LysoTracker Red in distinct, spherical organelles in CHO cells. The overlapping areas were mostly distributed near and around the nuclear membrane of the cells (Figure 7A,B). Both fluorescent peptides were also found to be randomly distributed in the cytoplasm of cells, sometimes in punctate, vesicle-liked structures (Figure 7A,B). The accumulation of both NLS-10R-p53^{tet} and 10R-p53^{tet} peptides in acidic compartments suggests that these peptides enter the endosomal/lysosomal pathway following clathrin-mediated endocytosis. The precise localization of the 10R-p53^{tet} peptide in CHO cells was further analyzed by transmission electron microscopy. More precisely, CHO cells were incubated with biotinylated 10R-p53^{tet} peptides. Routing of the peptide into cells was revealed using streptavidin−gold particles. The biotinylated 10R-p53^{tet} peptides were found to accumulate inside cell membrane invaginations within the first 30 min of incubation (Figure 8A) and subsequently into vesicular compartments (Figure 8B). After 3 h, gold particles could still be observed in vesicles near the nucleus with free gold particles also present in the cytosol and the nucleus of CHO cells (Figure 8C). The localization events observed by electron microscopy correlate with the results obtained from flow cytometry, confocal microscopy, and transfection experiments.

10R-p53^{tet} Peptides Localize to the Nucleus of Mammalian Cells. Confocal microscopy performed on viable, unfixed eukaryotic cells was used to further investigate the intracellular distribution of NLS-10R-p53^{tet} and 10R-p53^{tet} peptides inside cells. Specifically, the majority of fluorescein-labeled 10R-p53^{tet} peptides localized to the nucleus of CHO and Vero

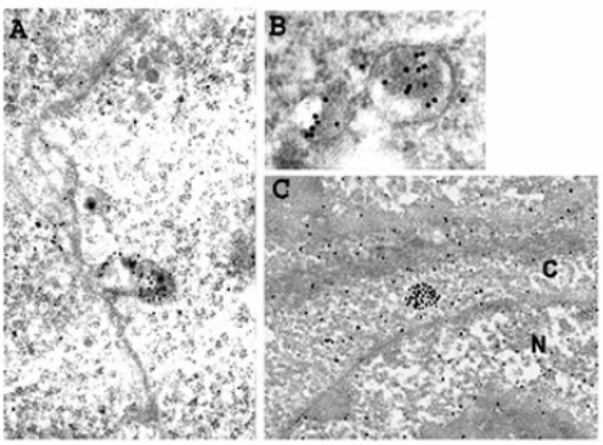

FIGURE 8: Localization of gold particle-labeled biotinylated 10R-p53^{tet} peptides in CHO cells as revealed by electron microscopy. Unfixed, viable CHO cells were treated with a biotinylated analogue of the tetrameric 10R-p53^{tet} peptide. The labeled cells were deposited on grids and subsequently treated with 15 nm colloidal gold−streptavidin particles. (A) An electron micrograph showing the biotinylated 10R-p53^{tet} peptide (dark spherical particles) clustered inside an invagination of the plasma membrane after a 30 min incubation at 37 °C. (B) Biotinylated 10R-p53^{tet} peptides trapped inside endocytic vesicles. (C) At 3 h postincubation, gold particle-labeled peptides are observed in the cytosol as well as in vesicles and in the nucleus of CHO cells.

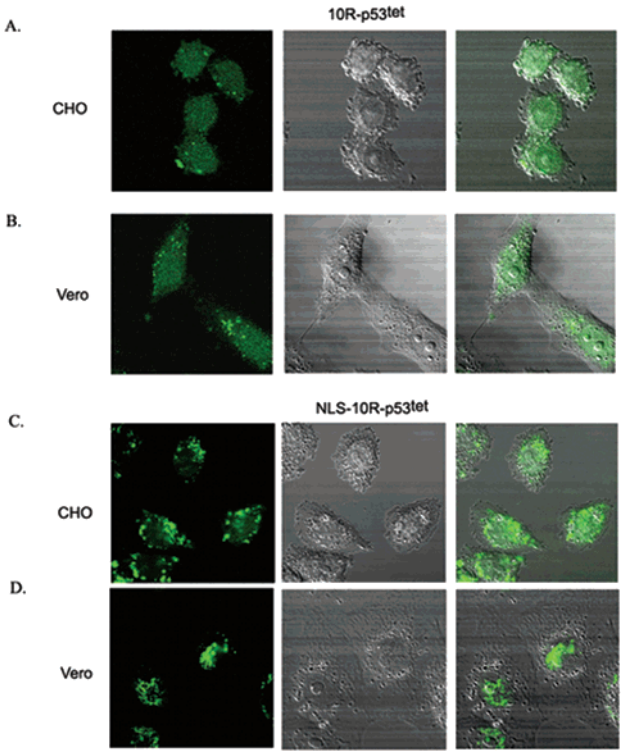

FIGURE 9: Confocal images depicting the localization of fluorescein-labeled NLS-10R-p53^{tet} and 10R-p53^{tet} peptides to the cell nucleus. (A and B) Unfixed, viable CHO or Vero cells were exposed to fluorescein-labeled 10R-p53^{tet} (1 μM) for 6 h at 37 °C, leading to the accumulation of green fluorescence in the nucleus. (C and D) Unfixed, viable CHO or Vero cells were exposed to fluorescein-labeled NLS-10R-p53^{tet} (1 μM) for only 1 h at 37 °C, suggesting a more rapid accumulation of green fluorescence in the nucleus than for the 10R-p53^{tet} peptide.

cells after incubation for 6 h at 37 °C (Figure 9A,B). Distinct spherical vesicles containing fluorescently labeled peptides could still be observed surrounding the nucleus (Figure 9A,B), suggesting that not all 10R-p53^{tet} peptides were able to escape from vesicular compartments. The fluorescein-labeled NLS-10R-p53^{tet} peptides localized to the nucleus of the CHO cells more rapidly than the 10R-p53^{tet} construct (incubation for 1 h at 37 °C; Figure 9C). The level of nuclear localization by NLS-10R-p53^{tet} peptides in Vero cells was lower, but aggregates of the fluorescein-labeled peptides could be observed inside the nucleus after incubation for just 1 h (Figure 9D). Again, endocytic vesicles trapping a large amount of fluorescein-labeled peptides could be observed in both CHO and Vero cells located at the periphery of the nuclear membrane (Figure 9C,D). Interestingly, it was observed that the removal of fluorescein-labeled 10R-p53^{tet} peptides from the extracellular medium of CHO cells following a 6 h "peptide loading" period results in the subsequent slow disappearance of cytosolic fluorescence but not of the peptide signal localized to the nucleus of cells (Supporting Information). This process of nuclear entrapment occurs despite the fact that the p53^{tet} domain itself encodes a nuclear export sequence (*11*).

DISCUSSION

H. Ryser demonstrated in a study published in 1965 that cationic peptides [polyornithine, polylysine, arginine-rich histones, spermine, and quaternary amine polymers (DEAE-dextran)] can direct the import of macromolecules such as proteins into eukaryotic cells (*56*). Subsequent investigations established a direct correlation linking the extent of cellular import of proteins to the molecular size of a cationic polymer (*16*, *57*). The empirical relationship led to the prediction that the minimal mass of a polycationic peptide needed to cause a nominal level of protein import into cells was on the order of ~500−900 Da, a molecular mass range corresponding to a peptide chain of approximately six or seven amino acids (*16*). Ryser did not provide evidence that short cationic peptides and in particular arginine peptides could represent effective protein transduction domains. This projection has instead been independently confirmed with the recent discovery that short arginine-rich peptide motifs present in proteins such as HIV Tat (*58*) and the *Drosophila antennapedia* homeodomain (*59*) can promote their cellular uptake. Cationic peptide sequences are now extensively used as protein transduction domains (PTDs) (*54*, *60*). More importantly, peptide dendrimers displaying multiple copies of such short cationic peptides (*9*, *15*) have recently been shown to mimic the dramatic enhancement in cellular uptake observed by Ryser for high-molecular mass, linear polycationic peptide conjugates (*61*). Similarly, the efficiency of nuclear import in proteins has been shown to increase with the number of nuclear localization signals (NLS) inserted into such conjugates (*14*).

The focus of this study was to assess the impact of peptide valency on the mechanisms of cellular entry and intracellular routing of cationic peptides in eukaryotic cells. Experimentally, self-assembling peptide dendrimers harboring cationic peptide motifs were designed and assembled by solid phase peptide synthesis to probe this effect. More specifically, a series of peptides were constructed in which one of three related classes of cationic sequences import signals, either 10 arginines (10R), 10 lysines (10K), or the HIV Tat peptide (Tat, GRKKRRQRRRAP, residues 48−59), was inserted at the N-terminus of the 31-residue tetramerization domain of human p53 (p53^{tet}, residues 225−255, Figure 1). Specific peptides also harbored the SV40 large T-antigen nuclear localization sequence (APPKKKRKVEDP, residues 124−135) for assessment of the routing of such peptides into the cell nucleus. All peptides were shown to assemble into tetramers in solution. These peptides were shown to be nontoxic to cells at doses as high as 25 μM and well above the concentrations used (0.1−0.5 μM) in these studies (Supporting Information). In addition, there were no observable phenotypic or morphological changes in CHO and Vero cells treated with these peptides. A parallel series of monomeric homologues of these synthetic peptides was also generated by introducing a single amino acid substitution within the p53^{tet} domain (L344P), a mutation that abolishes tetramer formation (*28*). The level of cellular import and nuclear localization was remarkable for tetrameric peptides, being 1−2 orders of magnitude greater than those of their monomeric equivalent peptides. The magnitude of these cell routing events was particularly impressive for the peptides containing decaarginyl sequences (Figures 2 and 3).

The mechanisms of cellular uptake and intracellular routing of these tetravalent peptide dendrimers into eukaryotic cells were then evaluated relative to their monomeric peptide homologues (Figures 2−6). The initial cellular import event for both monomeric and tetrameric arginine-rich p53^{tet} peptides, namely, 10R-p53^{tet} and NLS-10R-p53^{tet}, was their binding to anionic heparan sulfate (Figure 6). The selectivity of 10R-p53^{tet} and NLS-10R-p53^{tet} peptides for this class of surface proteoglycans is directly related to their cationic charges since polylysine (MW_{av} = 25 kDa) was shown to effectively inhibit their penetration into both CHO and Vero cells (Figure 5). These peptides were internalized via classical clathrin-coated pits (Figures 5 and 8) and subsequently routed through endosomal and lysosomal compartments (Figures 4 and 7). This proposed mode of binding and internalization of these multivalent 10R-p53^{tet} peptides conforms with recent findings showing that HIV Tat and Antp PTD are endocytosed via their binding to heparan sulfate on the cell surface (*62*, *63*) and parallels the import mechanism proposed for related arginine-rich HIV Tat and Antp PTDs associated with streptavidin (*52*) and larger molecular entities such as liposomes (*64*). Interestingly, both of these molecular cargos (streptavidin and liposomes) result in a polyvalent display of arginine-rich peptides (tetravalency in the case of biotinylated PTD peptides associated with steptavidin and self-aggregating lipids derivatized with an HIV Tat peptide). A brief analysis of published studies on macromolecules labeled with PTD peptides actually indicates that in many cases, these peptide domains were unknowingly presented in multiple copies as a consequence of the quaternary structure of their protein cargo itself or the strategy involved in linking them to macromolecules. More specifically, the HIV Tat protein itself (*65*), β-galactosidase (*66*), and full-length human p53 (*8*) represent examples of proteins containing or labeled with PTD peptides that exist either as dimers or tetramers in solution. Furthermore, the HIV Tat PTD motif, Antp peptide, polylysine, or polyarginine has been extensively used to deliver the reporter green fluorescent protein (eGFP) (*67*−*70*) and ovalbumin (*71*−*73*) into eukaryotic

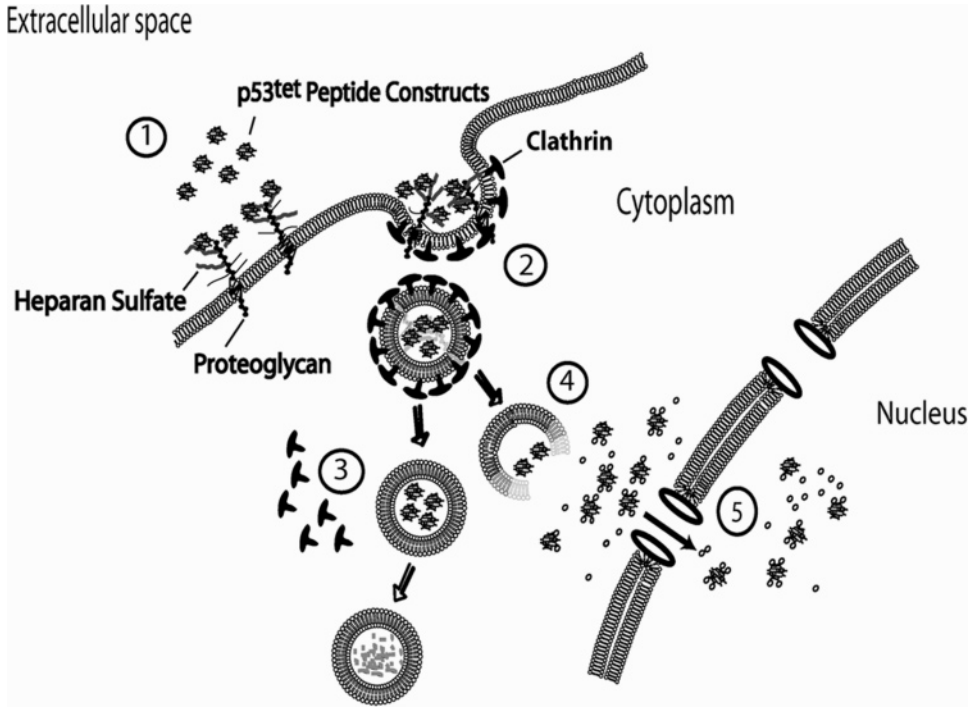

FIGURE 10: Postulated mechanisms of internalization and intracellular trafficking of tetravalent 10R-p53^{tet} peptides in eukaryotic cells. The results presented in this study support the view that the import and routing of multivalent arginine-rich p53^{tet} peptides into eukaryotic cells involve at least five routing events. These peptides bind initially to heparan sulfate on the cell surface (1), are subsequently imported into cells by clathrin-mediated endocytosis (2), are sorted through the endosomal/lysosomal vesicles, and are degraded or recycled out of the cell (3), with a fraction of the peptides escaping from acidic compartments (4) and reaching the cell nucleus (5).

cells. These proteins are known to exist as dimers and tetramers, respectively, in solution. Other examples of known multimeric proteins tagged with cationic import signals include oligoarginine conjugated to human catalase (*74*, *75*), a tetrameric protein, and polylysine conjugated to superoxide dismutase (Cu,Zn-SOD) (*76*), a dimeric protein.

The diagram presented in Figure 10 summarizes the entry and routing of 10R-p53^{tet} and NLS-10R-p53^{tet} peptides into cells as supported by the experimental evidence collected in this study.

Confocal (Figures 7 and 9) and electron microscopy (Figure 8) studies as well as transfection data (Figure 3 and the Supporting Information) indicate that a significant fraction of internalized 10R-p53^{tet} and NLS-10R-p53^{tet} peptides does reach the cytosol possibly as a result of escaping from endosomal or lysosomal compartments. The guanidinium group present on the side chain of arginines may provide a clue to this escape mechanism. More precisely, the acidic environment present in late endosome/lysosome vesicles results in a membrane potential that may favor the translocation of positively charged guanidinium-rich peptides to the less acidic cytosol (*73*). The guanidinium groups associated with short arginine-rich transporter peptides have been postulated to form hydrogen bond pairing interactions with vesicular membranes, an event that may trigger their export to the cytosol (*77*). Another intriguing finding is that depolymerizing F-actin with cytochalasin D allowed partial inhibition of the internalization of the decaarginyl peptides into both CHO and Vero cells (Figure 5). The uptake of an eight-residue arginine (R8) peptide by HeLa cells can also be inhibited by this depolymerizing agent (*78*). The report also stated that the import of R8 induced F-actin rearrangement inside HeLa cells, giving further credence to the involvement of the cytoskeleton in arginine-rich peptide transport.

The nuclear localization and nuclear retention of arginyl-p53^{tet} peptides into this organelle occurred in the presence or absence of the NLS sequence derived from the SV40 large T-antigen (Figures 7−9 and the Supporting Information). This nuclear localization signal has been shown to interact with the importin α/β-heterodimer and to facilitate nuclear import of proteins containing this sequence (*79*). In contrast, arginine-rich domains from HIV Tat and Rev proteins have been postulated to facilitate protein translocation into the nucleus through their interaction with importin β directly without any initial binding to importin α (*80*, *81*). This study highlights the fact that both 10R-p53^{tet} peptides accumulate inside the nucleus of CHO cells, with the difference that the NLS-containing variant enters the nucleus more quickly (within 1 h) than the construct harboring the 10-arginine sequence alone. Two points can be made from these observations. (1) Polyarginine sequences can act as signal sequence and direct nuclear import. (2) The combination of polyarginine sequence and a monopartite NLS can lead to rapid nuclear import. Hence, the observed difference in the rate of nuclear import between 10R-p53^{tet} and NLS-10R-p53^{tet} peptides may reflect the additive effects of the import arginyl sequence and the conventional monopartite NLS acting through distinct initial binding events with importin molecules.

ACKNOWLEDGMENT

We thank Steven Doyle and Battista Calvieri for their help in performing transmission electron microscopy, as well as James Jonkman for his assistance with confocal microscopy.

SUPPORTING INFORMATION AVAILABLE

Six additional figures. This material is available free of charge via the Internet at http://pubs.acs.org.

REFERENCES

1. Carman, C. V., and Springer, T. A. (2003) Integrin avidity regulation: Are changes in affinity and conformation underemphasized? *Curr. Opin. Cell Biol. 15*, 547−56.
2. Galustian, C., Childs, R. A., Yuen, C. T., Hasegawa, A., Kiso, M., Lubineau, A., Shaw, G., and Feizi, T. (1997) Valency dependent patterns of binding of human L-selectin toward sialyl and sulfated oligosaccharides of Le(a) and Le(x) types: Relevance to anti-adhesion therapeutics, *Biochemistry 36*, 5260−6.
3. Kentsis, A., Gordon, R. E., and Borden, K. L. (2002) Control of biochemical reactions through supramolecular RING domain self-assembly, *Proc. Natl. Acad. Sci. U.S.A. 99*, 15404−9.
4. Boraston, A. B., Bolam, D. N., Gilbert, H. J., and Davies, G. J. (2004) Carbohydrate-binding modules: Fine-tuning polysaccharide recognition, *Biochem. J. 382*, 769−81.
5. Feng, W., Long, J. F., Fan, J. S., Suetake, T., and Zhang, M. (2004) The tetrameric L27 domain complex as an organization platform for supramolecular assemblies, *Nat. Struct. Mol. Biol. 11*, 475−80.
6. John, S., Vinkemeier, U., Soldaini, E., Darnell, J. E., Jr., and Leonard, W. J. (1999) The significance of tetramerization in promoter recruitment by Stat5, *Mol. Cell. Biol. 19*, 1910−8.
7. Park, Y. C., Burkitt, V., Villa, A. R., Tong, L., and Wu, H. (1999) Structural basis for self-association and receptor recognition of human TRAF2, *Nature 398*, 533−8.
8. Chene, P. (2001) The role of tetramerization in p53 function, *Oncogene 20*, 2611−7.
9. Gariepy, J., and Kawamura, K. (2001) Vectorial delivery of macromolecules into cells using peptide-based vehicles, *Trends Biotechnol. 19*, 21−8.
10. Dingwall, C., Sharnick, S. V., and Laskey, R. A. (1982) A polypeptide domain that specifies migration of nucleoplasmin into the nucleus, *Cell 30*, 449−58.
11. Stommel, J. M., Marchenko, N. D., Jimenez, G. S., Moll, U. M., Hope, T. J., and Wahl, G. M. (1999) A leucine-rich nuclear export signal in the p53 tetramerization domain: Regulation of subcellular localization and p53 activity by NES masking, *EMBO J. 18*, 1660−72.
12. Liang, S. H., and Clarke, M. F. (1999) A bipartite nuclear localization signal is required for p53 nuclear import regulated by a carboxyl-terminal domain, *J. Biol. Chem. 274*, 32699−703.
13. Goldfarb, D. S., Gariepy, J., Schoolnik, G., and Kornberg, R. D. (1986) Synthetic peptides as nuclear localization signals, *Nature 322*, 641−4.
14. Dworetzky, S. I., Lanford, R. E., and Feldherr, C. M. (1988) The effects of variations in the number and sequence of targeting signals on nuclear uptake, *J. Cell Biol. 107*, 1279−87.
15. Sheldon, K., Liu, D., Ferguson, J., and Gariepy, J. (1995) Loligomers: Design of de novo peptide-based intracellular vehicles, *Proc. Natl. Acad. Sci. U.S.A. 92*, 2056−60.
16. Ryser, H. J. (1967) A membrane effect of basic polymers dependent on molecular size, *Nature 215*, 934−6.
17. Richard, J. P., Melikov, K., Vives, E., Ramos, C., Verbeure, B., Gait, M. J., Chernomordik, L. V., and Lebleu, B. (2003) Cell-penetrating peptides. A reevaluation of the mechanism of cellular uptake, *J. Biol. Chem. 278*, 585−90.
18. Fuchs, S. M., and Raines, R. T. (2004) Pathway for polyarginine entry into mammalian cells, *Biochemistry 43*, 2438−44.
19. Richard, J. P., Melikov, K., Brooks, H., Prevot, P., Lebleu, B., and Chernomordik, L. V. (2005) Cellular Uptake of Unconjugated TAT Peptide Involves Clathrin-dependent Endocytosis and Heparan Sulfate Receptors, *J. Biol. Chem. 280*, 15300−6.
20. Ferrari, A., Pellegrini, V., Arcangeli, C., Fittipaldi, A., Giacca, M., and Beltram, F. (2003) Caveolae-mediated internalization of extracellular HIV-1 tat fusion proteins visualized in real time, *Mol. Ther. 8*, 284−94.
21. Fittipaldi, A., Ferrari, A., Zoppe, M., Arcangeli, C., Pellegrini, V., Beltram, F., and Giacca, M. (2003) Cell Membrane Lipid Rafts Mediate Caveolar Endocytosis of HIV-1 Tat Fusion Proteins, *J. Biol. Chem. 278*, 34141−9.
22. Wadia, J. S., Stan, R. V., and Dowdy, S. F. (2004) Transducible TAT-HA fusogenic peptide enhances escape of TAT-fusion proteins after lipid raft macropinocytosis, *Nat. Med. 10*, 310−5.
23. Kaplan, I. M., Wadia, J. S., and Dowdy, S. F. (2005) Cationic TAT peptide transduction domain enters cells by macropinocytosis, *J. Controlled Release 10*, 247−53.
24. Locker, J. K., Kuehn, A., Schleich, S., Rutter, G., Hohenberg, H., Wepf, R., and Griffiths, G. (2000) Entry of the two infectious forms of vaccinia virus at the plasma membrane is signaling-dependent for the IMV but not the EEV, *Mol. Biol. Cell 11*, 2497−511.
25. Francis, C. L., Ryan, T. A., Jones, B. D., Smith, S. J., and Falkow, S. (1993) Ruffles induced by *Salmonella* and other stimuli direct macropinocytosis of bacteria, *Nature 364*, 639−42.
26. Alpuche-Aranda, C. M., Racoosin, E. L., Swanson, J. A., and Miller, S. I. (1994) *Salmonella* stimulate macrophage macropinocytosis and persist within spacious phagosomes, *J. Exp. Med. 179*, 10079−83.
27. Marechal, V., Prevost, M. C., Petit, C., Perret, E., Heard, J. M., and Schwartz, O. (2001) Human immunodeficiency virus type 1 entry into macrophages mediated by macropinocytosis, *J. Virol. 75*, 11166−77.
28. Davison, T. S., Yin, P., Nie, E., Kay, C., and Arrowsmith, C. H. (1998) Characterization of the oligomerization defects of two p53 mutants found in families with Li-Fraumeni and Li-Fraumeni-like syndrome, *Oncogene 17*, 651−6.
29. Esko, J. D., Stewart, T. E., and Taylor, W. H. (1985) Animal cell mutants defective in glycosaminoglycan biosynthesis, *Proc. Natl. Acad. Sci. U.S.A. 82*, 3197−201.
30. Lidholt, K., Weinke, J. L., Kiser, C. S., Lugemwa, F. N., Bame, K. J., Cheifetz, S., Massague, J., Lindahl, U., and Esko, J. D. (1992) A single mutation affects both *N*-acetylglucosaminyltransferase and glucuronosyltransferase activities in a Chinese hamster ovary cell mutant defective in heparan sulfate biosynthesis, *Proc. Natl. Acad. Sci. U.S.A. 89*, 2267−71.
31. Brokx, R. D., Bolewska-Pedyczak, E., and Gariepy, J. (2003) A stable human p53 heterotetramer based on constructive charge interactions within the tetramerization domain, *J. Biol. Chem. 278*, 2327−32.
32. Johnson, C. R., Morin, P. E., Arrowsmith, C. H., and Freire, E. (1995) Thermodynamic analysis of the structural stability of the tetrameric oligomerization domain of p53 tumor suppressor, *Biochemistry 34*, 5309−16.
33. Jeffrey, P. D., Gorina, S., and Pavletich, N. P. (1995) Crystal structure of the tetramerization domain of the p53 tumor suppressor at 1.7 angstroms, *Science 267*, 1498−502.
34. Lee, W., Harvey, T. S., Yin, Y., Yau, P., Litchfield, D., and Arrowsmith, C. H. (1994) Solution structure of the tetrameric minimum transforming domain of p53, *Nat. Struct. Biol. 1*, 877−90.
35. Mateu, M. G., Sanchez Del Pino, M. M., and Fersht, A. R. (1999) Mechanism of folding and assembly of a small tetrameric protein domain from tumor suppressor p53, *Nat. Struct. Biol. 6*, 191−8.
36. Davison, T. S., Nie, X., Ma, W., Lin, Y., Kay, C., Benchimol, S., and Arrowsmith, C. H. (2001) Structure and functionality of a designed p53 dimer, *J. Mol. Biol. 307*, 605−17.
37. Mateu, M. G., and Fersht, A. R. (1999) Mutually compensatory mutations during evolution of the tetramerization domain of tumor suppressor p53 lead to impaired hetero-oligomerization, *Proc. Natl. Acad. Sci. U.S.A. 96*, 3595−9.
38. Mateu, M. G., and Fersht, A. R. (1998) Nine hydrophobic side chains are key determinants of the thermodynamic stability and oligomerization status of tumour suppressor p53 tetramerization domain, *EMBO J. 17*, 2748−58.
39. Efthymiadis, A., Briggs, L. J., and Jans, D. A. (1998) The HIV-1 Tat nuclear localization sequence confers novel nuclear import properties, *J. Biol. Chem. 273*, 1623−8.
40. Kalderon, D., Richardson, W. D., Markham, A. F., and Smith, A. E. (1984) Sequence requirements for nuclear location of simian virus 40 large-T antigen, *Nature 311*, 33−8.
41. Furlanetto, R. W. (1988) Receptor-mediated endocytosis and lysosomal processing of insulin-like growth factor I by mitogenically responsive cells, *Endocrinology 122*, 2044−53.
42. Fischer, R., Köhler, K., Fotin-Mleczek, M., and Brock, R. (2004) A Stepwise Dissection of the Intracellular Fate of Cationic Cell-penetrating Peptides, *J. Biol. Chem. 279*, 12625−35.
43. Decorti, G., Malusa, N., Furlan, G., Candussio, L., and Klugmann, F. B. (1999) Endocytosis of gentamicin in a proximal tubular renal cell line, *Life Sci. 65*, 1115−24.

44. Deguchi, Y., Miyakawa, Y., Sakurada, S., Naito, Y., Morimoto, K., Ohtsuki, S., Hosoya, K., and Terasaki, T. (2003) Blood-brain barrier transport of a novel micro 1-specific opioid peptide, H-Tyr-D-Arg-Phe-β-Ala-OH (TAPA), *J. Neurochem. 84*, 1154−61.
45. Sai, Y., Kajita, M., Tamai, I., Wakama, J., Wakamiya, T., and Tsuji, A. (1998) Adsorptive-mediated endocytosis of a basic peptide in enterocyte-like Caco-2 cells, *Am. J. Physiol. 275*, G514−20.
46. Heuser, J. E., and Anderson, R. G. (1989) Hypertonic media inhibit receptor-mediated endocytosis by blocking clathrin-coated pit formation, *J. Cell Biol. 108*, 389−400.
47. Vandenbulcke, F., Nouel, D., Vincent, J. P., Mazella, J., and Beaudet, A. (2000) Ligand-induced internalization of neurotensin in transfected COS-7 cells: Differential intracellular trafficking of ligand and receptor, *J. Cell Sci. 113* (Part 17), 2963−75.
48. Okamoto, Y., Ninomiya, H., Miwa, S., and Masaki, T. (2000) Cholesterol oxidation switches the internalization pathway of endothelin receptor type A from caveolae to clathrin-coated pits in Chinese hamster ovary cells, *J. Biol. Chem. 275*, 6439−46.
49. Nabi, I. R., and Le, P. U. (2003) Caveolae/raft-dependent endocytosis, *J. Cell Biol. 161*, 673−7.
50. Engqvist-Goldstein, A. E., and Drubin, D. G. (2003) Actin assembly and endocytosis: From yeast to mammals, *Annu. Rev. Cell Dev. Biol. 19*, 287−332.
51. Ferrari, A., Pellegrini, V., Arcangeli, C., Fittipaldi, A., Giacca, M., and Beltram, F. (2003) Caveolae-mediated internalization of extracellular HIV-1 tat fusion proteins visualized in real time, *Mol. Ther. 8*, 284−94.
52. Console, S., Marty, C., Garcia-Echeverria, C., Schwendener, R., and Ballmer-Hofer, K. (2003) Antennapedia and HIV transactivator of transcription (TAT) "protein transduction domains" promote endocytosis of high molecular weight cargo upon binding to cell surface glycosaminoglycans, *J. Biol. Chem. 278*, 35109−14.
53. David, G., Bai, X. M., Van der Schueren, B., Cassiman, J. J., and Van den Berghe, H. (1992) Developmental changes in heparan sulfate expression: In situ detection with mAbs, *J. Cell Biol. 119*, 961−75.
54. Dietz, G. P., and Bahr, M. (2004) Delivery of bioactive molecules into the cell: The Trojan horse approach, *Mol. Cell. Neurosci. 27*, 85−131.
55. Suzuki, T., Futaki, S., Niwa, M., Tanaka, S., Ueda, K., and Sugiura, Y. (2002) Possible existence of common internalization mechanisms among arginine-rich peptides, *J. Biol. Chem. 277*, 2437−43.
56. Ryser, H. J., and Hancock, R. (1965) Histones and basic polyamino acids stimulate the uptake of albumin by tumor cells in culture, *Science 150*, 501−3.
57. Ryser, H. J. (1968) Uptake of protein by mammalian cells: An underdeveloped area. The penetration of foreign proteins into mammalian cells can be measured and their functions explored, *Science 159*, 390−6.
58. Vives, E., Brodin, P., and Lebleu, B. (1997) A truncated HIV-1 Tat protein basic domain rapidly translocates through the plasma membrane and accumulates in the cell nucleus, *J. Biol. Chem. 272*, 16010−7.
59. Derossi, D., Joliot, A. H., Chassaing, G., and Prochiantz, A. (1994) The third helix of the Antennapedia homeodomain translocates through biological membranes, *J. Biol. Chem. 269*, 10444−50.
60. Brooks, H., Lebleu, B., and Vives, E. (2005) Tat peptide-mediated cellular delivery: Back to basics, *Adv. Drug Delivery Rev. 57*, 559−77.
61. Shen, W. C., and Ryser, H. J. (1978) Conjugation of poly-L-lysine to albumin and horseradish peroxidase: A novel method of enhancing the cellular uptake of proteins, *Proc. Natl. Acad. Sci. U.S.A. 75*, 1872−6.
62. Tyagi, M., Rusnati, M., Presta, M., and Giacca, M. (2001) Internalization of HIV-1 tat requires cell surface heparan sulfate proteoglycans, *J. Biol. Chem. 276*, 3254−61.
63. Argyris, E. G., Kulkosky, J., Meyer, M. E., Xu, Y., Mukhtar, M., Pomerantz, R. J., and Williams, K. J. (2004) The perlecan heparan sulfate proteoglycan mediates cellular uptake of HIV-1 Tat through a pathway responsible for biological activity, *Virology 330*, 481−6.
64. Fretz, M. M., Koning, G. A., Mastrobattista, E., Jiskoot, W., and Storm, G. (2004) OVCAR-3 cells internalize TAT-peptide modified liposomes by endocytosis, *Biochim. Biophys. Acta 1665*, 48−56.
65. Frankel, A. D., Bredt, D. S., and Pabo, C. O. (1988) Tat protein from human immunodeficiency virus forms a metal-linked dimer, *Science 240*, 70−3.
66. Tomino, S., and Meisler, M. (1975) Biochemical and immunological studies of purified mouse β-galactosidase, *J. Biol. Chem. 250*, 7752−8.
67. Han, K., Jeon, M. J., Kim, S. H., Ki, D., Bahn, J. H., Lee, K. S., Park, J., and Choi, S. Y. (2001) Efficient intracellular delivery of an exogenous protein GFP with genetically fused basic oligopeptides, *Mol. Cells 12*, 267−71.
68. Caron, N. J., Torrente, Y., Camirand, G., Bujold, M., Chapdelaine, P., Leriche, K., Bresolin, N., and Tremblay, J. P. (2001) Intracellular delivery of a Tat-eGFP fusion protein into muscle cells, *Mol. Ther. 3*, 310−8.
69. Fittipaldi, A., Ferrari, A., Zoppe, M., Arcangeli, C., Pellegrini, V., Beltram, F., and Giacca, M. (2003) Cell membrane lipid rafts mediate caveolar endocytosis of HIV-1 Tat fusion proteins, *J. Biol. Chem. 278*, 34141−9.
70. Park, J., Ryu, J., Kim, K. A., Lee, H. J., Bahn, J. H., Han, K., Choi, E. Y., Lee, K. S., Kwon, H. Y., and Choi, S. Y. (2002) Mutational analysis of a human immunodeficiency virus type 1 Tat protein transduction domain which is required for delivery of an exogenous protein into mammalian cells, *J. Gen. Virol. 83*, 1173−81.
71. Kim, D. T., Mitchell, D. J., Brockstedt, D. G., Fong, L., Nolan, G. P., Fathman, C. G., Engleman, E. G., and Rothbard, J. B. (1997) Introduction of soluble proteins into the MHC class I pathway by conjugation to an HIV tat peptide, *J. Immunol. 159*, 1666−8.
72. Pietersz, G. A., Li, W., and Apostolopoulos, V. (2001) A 16-mer peptide (RQIKIWFQNRRMKWKK) from antennapedia preferentially targets the class I pathway, *Vaccine 19*, 1397−405.
73. Moy, P., Daikh, Y., Pepinsky, B., Thomas, D., Fawell, S., and Barsoum, J. (1996) Tat-mediated protein delivery can facilitate MHC class I presentation of antigens, *Mol. Biotechnol. 6*, 105−13.
74. Watanabe, N., Iwamoto, T., Bowen, K. D., Dickinson, D. A., Torres, M., and Forman, H. J. (2003) Bio-effectiveness of Tat-catalase conjugate: A potential tool for the identification of H_2O_2-dependent cellular signal transduction pathways, *Biochem. Biophys. Res. Commun. 303*, 287−93.
75. Jin, L. H., Bahn, J. H., Eum, W. S., Kwon, H. Y., Jang, S. H., Han, K. H., Kang, T. C., Won, M. H., Kang, J. H., Cho, S. W., Park, J., and Choi, S. Y. (2001) Transduction of human catalase mediated by an HIV-1 TAT protein basic domain and arginine-rich peptides into mammalian cells, *Free Radical Biol. Med. 31*, 1509−19.
76. Park, J., Ryu, J., Jin, L. H., Bahn, J. H., Kim, J. A., Yoon, C. S., Kim, D. W., Han, K. H., Eum, W. S., Kwon, H. Y., Kang, T. C., Won, M. H., Kang, J. H., Cho, S. W., and Choi, S. Y. (2002) 9-Polylysine protein transduction domain: Enhanced penetration efficiency of superoxide dismutase into mammalian cells and skin, *Mol. Cells 13*, 202−8.
77. Rothbard, J. B., Jessop, T. C., Lewis, R. S., Murray, B. A., and Wender, P. A. (2004) Role of membrane potential and hydrogen bonding in the mechanism of translocation of guanidinium-rich peptides into cells, *J. Am. Chem. Soc. 126*, 9506−7.
78. Nakase, I., Niwa, M., Takeuchi, T., Sonomura, K., Kawabata, N., Koike, Y., Takehashi, M., Tanaka, S., Ueda, K., Simpson, J. C., Jones, A. T., Sugiura, Y., and Futaki, S. (2004) Cellular uptake of arginine-rich peptides: Roles for macropinocytosis and actin rearrangement, *Mol. Ther. 10*, 1011−22.
79. Makkerh, J. P., Dingwall, C., and Laskey, R. A. (1996) Comparative mutagenesis of nuclear localization signals reveals the importance of neutral and acidic amino acids, *Curr. Biol. 6*, 1025−7.
80. Palmeri, D., and Malim, M. H. (1999) Importin β can mediate the nuclear import of an arginine-rich nuclear localization signal in the absence of importin α, *Mol. Cell. Biol. 19*, 1218−25.
81. Truant, R., and Cullen, B. R. (1999) The arginine-rich domains present in human immunodeficiency virus type 1 Tat and Rev function as direct importin β-dependent nuclear localization signals, *Mol. Cell. Biol. 19*, 1210−7.

BI051338E